European Polymer Journal 106 (2018) 92–101

Contents lists available at ScienceDirect

European Polymer Journal

journal homepage: www.elsevier.com/locate/europolj

Macromolecular Nanotechnology

Synthesis of polyethylene/silica-silver nanocomposites with antibacterial properties by *in situ* polymerization

Giovani Pavoski[a], Renan Kalikoski[a], Gustavo Souza[a], Luiz Fernando Wentz Brum[a], Cristiane dos Santos[a], Ahmad Abo Markeb[b], João Henrique Zimnoch dos Santos[a], Xavier Font[b], Ignacio dell'Erba[c], Griselda Barrera Galland[a,*]

[a] *Instituto de Química, Universidade Federal do Rio Grande do Sul, 91501-970 Porto Alegre, RS, Brazil*
[b] *Institut de Ciência i Tecnologia Ambientais – Universitat Autònoma de Barcelona Building Z Campus UAB 08193 Bellaterra (Cerdanyola), Barcelona, Spain*
[c] *Institute of Materials Science and Technology (INTEMA), University of Mar del Plata and National Research Council (CONICET), Av. J. B. Justo 4302, 7600 Mar del Plata, Argentina*

ARTICLE INFO

Keywords:
Silver nanoparticles
Polymerization
Nanocomposites

ABSTRACT

Synthesis of polyethylene/silica-silver nanocomposites (PE/SiAg) by *in situ* polymerization with supported and non-supported catalysts was achieved using the Cp_2ZrCl_2/MAO catalytic system. Silica-silver nanoparticles (SiAg) were synthesized via two routes (acidic and basic) and characterized to determine the silver content, morphology, and size. The basic route resulted in particles with a lower concentration of silver and with smaller diameters. The polymerizations of ethylene in the presence of the fillers produced high yields of nanocomposites. The catalyst support in SiAg was efficient, although the percentage of Zr effectively immobilized was very low. Polyethylene melting and crystallization temperatures did not change significantly with the addition of the filler. SEM images showed differences in the morphologies between the supported and non-supported catalysis, and between the acidic and basic conditions for SiAg preparation. Two different tests were performed and showed that the nanocomposites inhibited the proliferation of bacteria in contact with the films.

1. Introduction

Nanotechnology is an emerging scientific field that has potential to generate new and innovative materials [1–3]. Nanomaterials may provide solutions to technological and environmental challenges in the areas of solar energy conversion, catalysis, water treatment and medicine [4,5].

Polymer nanocomposites are advanced functional materials composed of nanoparticles dispersed in a polymeric matrix [6]. In recent decades, much research has been carried out into different polymer matrices (polyethylene, polypropylene, polyvinyl acetate, etc) and nanofillers (graphene, silver, gold, clays, silica, etc) [7–10]. One important application of polymer nanocomposites is in antimicrobial materials, not only in medical applications such as catheters, cannulas, and prostheses, but also in food packaging [11]. Recently, safe, biocompatible inorganic antibacterial nanoparticles with high stability under processing conditions, such as metals and metal oxides, have been preferred to organic antibiotics due to microbial resistance to the continuous use of organic products [12–14].

High density polyethylene (HDPE) is an inert and hydrophobic material with low price, low weight and easy to process that does degrade in vivo and it is already used in medical applications where a durable material is needed. In this sense it is used for packaging of drugs and devices, inner lining of catheters or as graft for craniofacial contour augmentation in medicine [15].

Silver, as a non-specific biocidal agent, acts strongly against a broad spectrum of bacterial and fungal species, including antibiotic-resistant strains [16], and has been investigated by several researchers in recent years [17–21]. Tamayo et al. [22] studied the antibacterial properties of polyethylene/silver and polyethylene/copper nanocomposites against *Listeria monocytogenes*. Both nanocomposites showed excellent antibacterial activity. In another study, Zheng [23] prepared films of polyethylene/AgNPs (silver nanoparticles), that were shown to be effective in killing *Bacillus cereus* (Gram-positive) and *Escherichia coli* (Gram-negative) bacteria. However, for practical applications such as antibacterial coatings or films to protect food, it is useful to produce AgNPs covalently bonded to an adequate support. In this way, the AgNPs are retained in the polymer and at the same time maintain their

* Corresponding author.
E-mail address: griselda.barrera@ufrgs.br (G.B. Galland).

https://doi.org/10.1016/j.eurpolymj.2018.07.011
Received 28 May 2018; Received in revised form 2 July 2018; Accepted 8 July 2018
Available online 09 July 2018
0014-3057/ © 2018 Elsevier Ltd. All rights reserved.

antibacterial activity.

Nanoparticles are difficult to disperse in polymers because they tend to agglomerate and the metals oxidize. A strategy to solve these problems is the encapsulation or bonding to inert fillers, for example, silica. The preparation of Ag NPs-modified silica can be achieved by grafting [24] or the sol-gel method. In the grafting method, there is a direct link between the support and the AgNPs. DelÍErba et al. [25] succeeded in synthesizing AgNPs using glycerol as both solvent and reducing agent, and (3-aminopropyl)trimethoxysilane (APTMS) as stabilizer. They produced AgNPs that were covalently bonded to the surface of a colloidal silica by hydrolysis/condensation between the terminal Si-O-CH_3 groups of the stabilizer and the superficial Si-OH groups of silica. This colloidal silica decorated with AgNPs showed antibacterial activity in cultures of *E. coli*.

Nanocomposites can be prepared by direct mixing of the nanoparticles and the polymer (solution intercalation, melt intercalation) or by *in situ* synthesis, where polymerization of the monomer takes place in the presence of the nanoparticles (*in situ* intercalative polymerization or polymerization with the supported catalyst) [26]. The direct mixing of nanoparticles with the polymer is very simple, but it can easily induce aggregation of the nanoparticles [27,28]. On the other hand, *in situ* polymerization tends to improve the properties of the nanocomposites due to better dispersion of the nanofiller [29].

The catalysts most widely used in the industrial production of polyethylene are Ziegler-Natta catalysts followed by the metallocenes. Metallocene complexes have made important contributions to the polyolefin field [30], by producing polymers with new properties and new applications due to the control of molar mass and co-monomer distributions [31–33]. Supported metallocenes have been investigated over the last 30 years. Many routes to immobilization have been proposed, leading to different catalytic activity and polymer properties [34,35]. Generally, polymers produced with supported metallocenes have a higher average molecular weight due to a reduction in the rate of termination reactions [36–39] and a controlled morphology. The immobilization of metallocene catalysts on supports is an alternative approach for utilization of the metallocene catalysts in industrial plants [40].

To improve the antimicrobial efficiency of these polymeric nanocomposites, the distribution of the nanoparticles is important, as well as several other crucial parameters, including: particle size, degree of particle agglomeration, silver content, and interaction of the silver surface with the polymer host [11].

In this study, we focused on the synthesis of nanocomposites by *in situ* polymerization of ethylene with a non-supported and supported metallocene catalyst. Silver nanoparticles covalently bonded to the surface of a colloidal silica was used as filler. The same silica containing the AgNPs was used as the support for the catalyst [41–43]. The main objective was to obtain good distribution of the SiAg nanoparticles in the polymer matrix, preserving the properties of the polymer and increasing the antibacterial action of the nanocomposite.

2. Experimental

2.1. Materials

A new synthesis of the silver nanoparticles bonded to silica (SiAg) via the basic route was reported by dell'Erba [25]. Silver nanoparticles (Ag NPs) were obtained by reducing silver nitrate ($AgNO_3$, ACS reagent, purity > 99%, Sigma-Aldrich) with anhydrous glycerol (Cicarelli, 99.5%), in the presence of 3-aminopropyl trimethoxysilane (APTMS, purity > 97%, Fluka) as a stabilizer, as reported by dell'Erba. Briefly, 75 mg of $AgNO_3$ were dissolved in 1.5 g of anhydrous glycerol with stirring at 50 °C. Then, the appropriate amount of APTMS was added and the reaction was conducted during 1 h. Three molar ratios were used (APTMS/Ag = 2, 4, and 8), and the resulting Ag NPs were named Ag2, Ag4, and Ag8, respectively. The covalent bonding of Ag NPs to the colloidal silica was achieved by two routes: basic (NaOH) and acidic (HCOOH). The colloidal dispersion of Ag NPs (1.5 g) in glycerol was washed three times with tetrahydrofuran (THF, Cicarelli), a solvent that is immiscible with glycerol, in order to remove residual APTMS not bonded to the NPs. Then, 1 g of commercial colloidal silica (Aerosil OX 50, Degussa, specific area of 50 $m^2\,g^{-1}$ with approximately 6.10^{-6} mol OH/m^2) was added together with 5 mL of THF and 0.5 mL of aqueous 0.02 M NaOH (basic route) or 0.05 mL 85% HCOOH (acidic route), with vigorous stirring. After reacting for 24 h, the slurry was washed with water and centrifuged at 6000 rpm for 5 min. This process was repeated several times until the supernatant was completely transparent. The solid product was then dried at 110 °C for 2 h and ground. A blank test was also carried out on silica following exactly the same procedure employed in the basic route but omitting the addition of Ag NPs.

Polymerization reactions were performed in a 100 mL reactor (Parr Instrument Company, Illinois, USA). The solvents and solutions used in the polymerization reactions were handled under an inert atmosphere of argon using the standard Schlenk technique. The reagents were used as received, except toluene (Nuclear, Brazil), which was distilled under argon with metallic sodium and benzophenone (Sigma-Aldrich, Brazil). [44] The metallocene catalyst used was bis(cyclopentadienyl)zirconium (IV) dichloride (Cp_2ZrCl_2) and the co-catalyst was 10% methylaluminoxane solution (MAO), both from Sigma-Aldrich.

2.2. Polymerization reactions with a non-supported catalyst

Polymerization reactions were performed in a 100 mL reactor. Toluene as the solvent and MAO (Al/Zr = 1000) as co-catalyst and scavenger were first added to the reactor. Then, a suspension of SiAg in toluene was added, and 4.10^{-6} mol of the catalyst, Cp_2ZrCl_2, when using 50 mg of SiAg, and 2.10^{-5} mol when using 100 mg of SiAg. The reactions were performed at 50 °C using 3.0 bar ethylene pressure for 30 min. The polymerization reactions were stopped using ethanol acidified with HCl (10%).

2.3. Polymerization reactions with a supported catalyst

SiAg (50 mg or 100 mg) was placed in a Schlenk vessel with toluene under an inert atmosphere. Then, MAO (Al/Zr = 1000) was added to the SiAg and stirred with a magnetic bar for 15 min. Next, Cp_2ZrCl_2 was added (4.10^{-6} mol for 50 mg SiAg or 2.10^{-5} mol for 100 mg SiAg), and the suspension was stirred for 2 h at 50 °C. The suspension was decanted and the supernatant removed, the solid was then washed three times with toluene. Thereafter, SiAg/MAO/Cp_2ZrCl_2 was used as the catalyst for the polymerization reaction. The reactions were performed as described with the non-supported catalyst, but in the reactor, only 0.1 mL of MAO was added to remove any impurities from the reactor.

2.4. Characterization

The concentration of Ag nanoparticles, and the concentration of Zr on the support, were determined by inductively coupled plasma optical emission spectrometry (ICP) using a Perkin Elmer, Optima 7300 instrument.

Small angle X-ray scattering measurements were conducted at 1.55 Å wavelength, with a source-to-detector distance of 1595.0 mm, at the Brazilian Synchrotron Light Laboratory (LNLS, Campinas, Brazil) using the D11A-SAXS1 line of a synchrotron source. Scattering profiles were fit using the Irena evaluation routine [45] implemented using Igor Pro Software (WaveMetrics, Portland, OR, USA) [46]. A multilevel unified fit was used to describe one or two levels of structural organization from the scattering profile data [46,47]. The particle diameters were calculated according to Eq. (1).

$$Dp = 2 \cdot Rg \cdot \left(\frac{5}{3}\right)^{0.5} \quad (1)$$

The specific surface area, pore size, and pore volume were determined by Nitrogen Porosimetry, obtained from nitrogen adsorption–desorption isotherms at −196 °C. The samples (100–200 mg) were kept at 110 °C for 18 h under vacuum before each measurement (Micromeritics Vac Prep 061). The nitrogen adsorption isotherms were measured using a Micromeritics TriStar II 3020 system in the partial pressure range of $0.01 < P/P_0 < 0.25$. The specific surface area (S_{BET}) was calculated using the Brunauer–Emmett–Teller method (BET) [48,49], and the pore diameter (Dp_{BJH}) and pore volume (Vp_{BJH}) were calculated from the cumulative desorption curve using the Barret–-Joyner–Halenda (BJH) algorithm [50].

Thermogravimetric analysis (TGA) was performed on an SDT Q600 thermal analyzer Q20 (TA Instruments) at a scanning rate of 20 °C/min from 25 to 700 °C.

The melting temperature and crystallinity of the nanocomposites were measured using a differential scanning calorimeter (TA Instruments Q20) with a heating rate of 10 °C/min and a temperature range of 20–160 °C in air atmosphere. The heating cycle was performed twice to remove the thermal history of the material, and only the results of the second heating were considered. The equipment was first calibrated with Indium standard at the same heating rate. The samples (1.5–2.5 mg) were analyzed in aluminum pans. The crystallinities of the polymers were calculated from Eq. (2):

$$Xc = \frac{\Delta Hf}{\Delta Hf^{\circ}} \times 100 \quad (2)$$

in which Xc represents the crystallinity content, ΔHf is the heat of fusion of the sample (area of the endothermic curve) and ΔHf° is the heat of fusion of 100% crystalline polyethylene (64.5 cal g^{-1} or 293.9 J g^{-1}) [51].

Scanning electron microscopy (SEM) was performed using a Carl Zeiss (model EVO MA10) operating at 7 and 15 kV, with aluminum stubs and gold metallization. The antibacterial activities were determined using *Salmonella* spp. (Gram negative), *Staphylococcus aureus* (Gram positive), and *Escherichia coli* (Gram negative). Two different antibacterial tests were done.

The water contact angle test was carried out using the sessile drop method, where a drop of 2 μL of deionized water at room temperature was steadily deposited on the surface of the neat PE matrix and its nanocomposites, using a microsyringe. The images were captured using "Drop Shape Analysis system" equipment, Kruss, DSA. Each measurement was repeated at least five times at different positions. A digital video camera was used to capture the images that were analyzed by Surftens 3.0 software for contact angle measurements.

Test One involved the disc diffusion (20 mm diameter film discs placed on agar gel) and agar well (7 mm diameter holes cut into the agar gel) methods were used for films of nanocomposites and nanoparticles, respectively. Bacteria were cultured in brain heart infusion (BHI) broth at 37 °C. A bacterial lawn culture was prepared by spreading 100 mL culture broth (10^7 CFU/mL) for each test organism on solid BHI agar plates using the swab technique. Contact time was 24 h at a temperature of 37 °C. Each experiment was made in duplicate.

Test Two involved contact between the liquid culture medium and the nanoparticles and films. The medium used was Luria-Bertani (LB) (10 g tryptone, 5 g yeast extract, 10 g NaCl in 1 L of distilled water) [52]. The pH was adjusted to 7 with concentrated NaOH. The medium with all the materials used were autoclaved. For the test using 2 mL of LB, the incubation was performed on a commercial Cell Culture Plate (SPL Life Sciences Co., Ltd). The concentration of the bacteria was measured by optical density at a wavelength of 600 nm. Both tests One and Two were used for nanoparticles and nanocomposites (film).

3. Results and discussion

In the first part of this study, we characterized the colloidal silica bonded to AgNPs (SiAg). The synthesis of these particles via the basic route has already been described [24], but in this work the particles were also obtained via the acidic route. The AgNPs differed due to the ratio of stabilizer/silver that was used APTMS/Ag = 2, 4, and 8 named AgNP2, AgNP4 and AgNP8, and resulted in different AgNP sizes between 10 and 50 nm (AgNP2 > AgNP4 > AgNP8) as shown by TEM in Ref. [24]. ICP-OES was used to investigate the amount of silver in the SiAg samples and to analyze the ability of the acidic and basic routes to incorporate Ag in silica. The results are shown in Table 1.

Table 1
ICP-OES analysis for the determination of silver content, SAXS for determination of particle diameter, and the Porod law (ρ) in the SiAg nanoparticles.

Sample	Route	%wt.-Ag	Rg2 (nm)[a]	Dp2 (nm)[b]	ρ
SiAg2	NaOH	0.510 ± 0.013	12.71	32.82	3.12
SiAg4	NaOH	0.621 ± 0.0414	7.78	20.09	3.22
SiAg8	NaOH	0.860 ± 0.120	7.17	18.51	3.10
SiAg2	HCOOH	2.420 ± 0.180	14.31	36.95	2.40
SiAg4	HCOOH	2.449 ± 0.0484	17.90	46.22	2.20
SiAg8	HCOOH	1.804 ± 0.307	11.80	30.47	2.95

[a] Radius of gyration of the secondary particle.
[b] Diameter of the secondary particle.

The results show that the acidic route incorporates approximately 4–5 times more Ag than the basic route. This can be explained by the mechanisms of the two routes [53]. The acidic catalysis between the methoxy group of APTMS and the silanol groups on the surface of the silica is faster than the basic one. This favors growth of the particle and the amount of AgNP in the nanoparticles. The covalent bonding of AgNPs to the silica surface was shown in Ref. [23], and revealed the generation of covalent Si-O-Si bonds between the silica surface and the aminosilane stabilizer. Lu et al. [54] demonstrated that the particle sizes of the silica over a wide range (30–280 nm), were controlled by simply adjusting the pH of the precursor solutions. In other work, Qiao et al. found that the particle size tended to increase from 30 to 85 nm, as the pH values decreased from 10 to 6.28 [55]. These previous reports show that the minimum particle size can be obtained at around pH 9–10, indicating that the rates of condensation, rather than the rates of hydrolysis, of the silica precursors highly affect the final particle size.

Increasing the APTMS/Ag ratios of the NPs (Ag2, Ag4, and Ag8) induced a decrease in the nanoparticles size via the basic route, but showed a slight increase in the Ag content from 0.51 to 0.86 wt%. However, increasing the APTMS/Ag ratios does not seem to affect the Ag content in the acidic route. In this case, the amount of Ag seems to be proportional to the particle size. It appears that the route (acidic or basic) influences the amount of Ag significantly more than the APTMS/Ag ratio.

Generally, the morphology and surface area of the silica changes with the type of synthesis. Therefore, the ICP-OES results are consistent with larger particle sizes incorporating more silver. As a result, the size and morphology of the silica particles were also studied.

Small-angle X-ray scattering (SAXS) was done to determine multiscale structure and fractal fracture of the SiAg nanoparticles. These determinations provide the particle diameter and Porod law. The results are also shown in Table 1. The X-ray scattering intensity profiles were used to analyze the differences in electron densities between the nanoparticles, the particle growth model, and the organization of the fractals of the particles into hierarchical multilevels [46,55]. The radius of gyration (Rg) and the fractal dimensions were obtained through the unified approach [56–59] in the power-law regions.

The results for Rg and particle diameter (Dp2) show that pH affects the particle size. The acidic route resulted in greater particle sizes than the basic route. From the results, we can confirm that the type of silica synthesis, acidic or basic, affects the structural organization of the nanoparticle, showing variations in particle scattering intensity.

The results of Porod law (ρ) also showed differences between the routes. A value for ρ of $1 < \rho < 2$ indicates a mass fractal structure,

Table 2
BET isotherm parameters: specific surface area, pore volume, and average desorption pore diameter for SiAg.

Sample		S_{BET} ($m^2.g^{-1}$)	Vp_{BJH} ($cm^3.g^{-1}$)	Dp_{BJH} (Å)
Blank Test*	NaOH	37	0.12	127
SiAg2	NaOH	37	0.11	107
SiAg4	NaOH	40	0.13	114
SiAg8	NaOH	39	0.12	116
SiAg2	HCOOH	35	0.10	102
SiAg4	HCOOH	35	0.09	104
SiAg8	HCOOH	36	0.10	105

$2 < \rho < 3$ indicates a fractal surface, and $\rho \leq 4$ a spherical particle. For all particles obtained via the basic route (NaOH), ρ values indicated spherical particles (3.10, 3.22, and 3.12). However, for the particles obtained via the acidic route, ρ indicated a fractal surface (2.95, 2.20, and 2.40). The basic route achieves smaller spherical shapes with increased surface area. However, the acidic route can lead to agglomeration, giving amorphous particles with low surface area [60]. The SAXS curves showed no variations, all followed the same decreasing pattern.

The results for specific surface area, pore volume, and pore diameter were also verified by Nitrogen Porosimetry. Table 2 and Fig. 1 show the adsorption–desorption isotherms and pore-size distribution of the synthesized SiAg.

Silica obtained using the sol-gel method can achieve surface areas of 285.8–363.3 $m^2\,g^{-1}$ [60], and by the grafting method they tend to remain the same as the silica that has been used. Therefore, the results for specific surface area for all SiAg particles may be considered low, but this is expected due to the silica used in the synthesis (Aerosil OX 50 with a specific area of 50 $m^2\,g^{-1}$). The acidic route, as expected from the previous analysis, gave particles with lower surface areas than those from the basic route. Consequently, the pore volume and diameter were also smaller in the acidic route. However, the pore diameter of the blank test was significantly higher suggesting that in the SiAg particles, the pores are occupied by Ag nanoparticles.

Depending on the process of the introduction of metal nanoparticle in silica (grafting or sol-gel) superficial area, pore volume and diameters can change or not. An example is given by Bernardes et al. [61] which synthesized silica with some metal oxides by non-hydrolytic sol–gel method and the surface area of the silica rose from 39 $m^2\,g^{-1}$ to a range of 188–415 $m^2\,g^{-1}$. These results are different from those of SiAg, where Ag is covalently bonded to silica, in which the surface area does not vary significantly (35–40 $m^2\,g^{-1}$). However, the pore diameter changed, decreasing after the binding of the AgNPs with the silica going from 127 Å to 102–116 Å. In this case it was used the grafting process in which the reaction is done over the surface and not inside the silica.

The results of nitrogen adsorption-desorption curves of the SiAg showed no differences compared to the data obtained from commercial silica (blank) indicating a mesoporous silica [62].

In the study by delÍErba [25], SiAg obtained via the basic route showed antibacterial activity against *Escherichia coli*. We studied the antibacterial activity of SiAg nanoparticles obtained by the acid route (HCOOH) using the Test One. The images of the antibacterial tests are shown in Fig. 2.

The inhibition zone for SiAg2 HCOOH was 18 mm, SiAg4 HCOOH

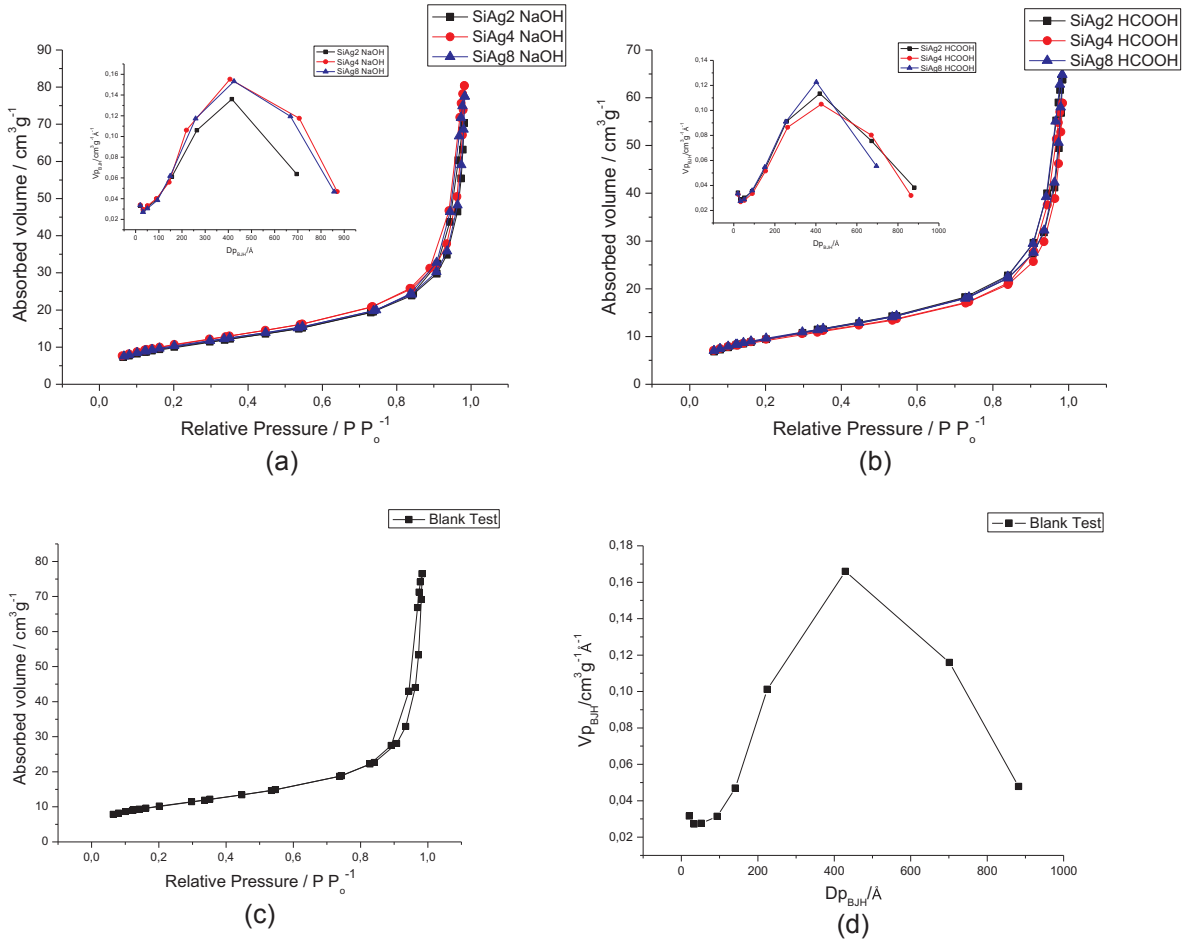

Fig. 1. Comparison of the N_2 adsorption–desorption isotherms for the synthesized SiAg nanoparticles. Inset: BJH pore-size distributions (Dp_{BJH}). Blank test was done with Aerosil OX-50 (Degussa) colloidal silica.

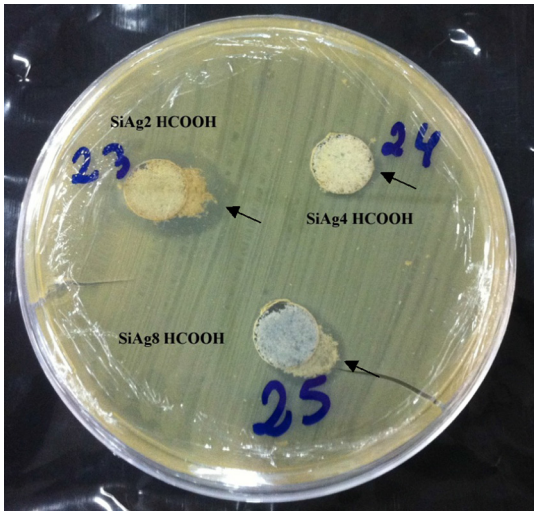

Fig. 2. Antibacterial activity of SiAg HCOOH nanoparticles against *E. coli* tested using the disc diffusion method.

13 mm, and SiAg8 HCOOH 15 mm, showing antibacterial activity for all SiAg nanoparticles. The highest antibacterial effect was shown by SiAg2 nanoparticles that have a high amount of Ag (2.42%) and a smaller size (36.9 nm). Despite SiAg4 having a good amount of Ag (2.44%), it has the biggest size (46.22 nm), which can hinder bacterial penetration.

Test Two (see experimental section), in which the films and the LB medium were in contact, was used for all nanoparticles. The results are shown in Table 3.

The results show that the routes (NaOH and HCOOH) give different bacterial inhibition. The basic route proved to be more efficient as it was able to inhibit bacterial growth by > 50%. In the acidic route, this value was < 50%. This may be explained by the nature of the silica-NPs. As already shown by BET and SAXS the NPs of the basic route are smaller and more spherical with a larger surface area. Thus, even though they possess a lower concentration of silver than NPs of the acidic route, their efficiency in inhibiting the growth of *E. coli* is greater.

These antimicrobial SiAg nanoparticles can be used as fillers in polymers. In this part of the study we prepared polyethylene/SiAg nanocomposites by *in situ* polymerization using two synthetic methods. In the first, we treated the SiAg NPs with the co-catalyst (MAO) to prevent deactivation of the metallocene catalyst by the oxygen functional groups in silica. Then, this suspension was added directly to the reactor with the other reagents. In the second method, we first supported the catalyst and co-catalyst on the SiAg nanoparticles to ensure that polymerization occurred from the nanoparticles. This second method was tested because it is the most suitable for industrial production of polyethylene.

The quantity of Zr in the supported catalysts was calculated by ICP, and the results are shown in Table 4. Considering that 2.42 wt% Zr was placed over the SiAg support, the amount of Zr immobilized on the SiAg NPs was very low.

Table 3
Antibacterial activity of SiAg nanoparticles tested against *Escherichia coli*, using 20 mg of sample in plates with 2 mL wells.

Route	Samples	Results	% of growth
NaOH	Control	1.54	100
	SiAg2	0.500	32.6
	SiAg4	0.745	48.5
	SiAg8	0.766	49.9
HCOOH	Control	1.06	100
	SiAg2	0.620	58.5
	SiAg4	0.930	87.7
	SiAg8	0.970	91.5

Table 4
ICP-OES results for the Zr support system.

Support	% wt.- Zr
SiAg2 NaOH/MAO/Cp_2ZrCl_2	0.0901 ± 0.0168
SiAg4 NaOH/MAO/Cp_2ZrCl_2	0.1209 ± 0.0185
SiAg8 NaOH/MAO/Cp_2ZrCl_2	0.0964 ± 0.0274
SiAg2 HCOOH/MAO/Cp_2ZrCl_2	0.0702 ± 0.0076
SiAg4 HCOOH/MAO/Cp_2ZrCl_2	0.0961 ± 0.0102
SiAg8 HCOOH/MAO/Cp_2ZrCl_2	0.0869 ± 0.0087

Table 5 shows the results of the polymerization of ethylene by both methods, with the non-supported and supported catalyst on SiAg. The results of the homogeneous polymerization of ethylene (without filler) are also shown. All polymerization reactions gave high yields and catalytic activities. As the results were similar to those obtained from the polymerization of ethylene, it can be concluded that the filler does not deactivate the catalyst. The yields from the supported reactions were slightly inferior to the non-supported reactions, but the catalytic activities were significantly higher. This shows that despite the low amount of Zr immobilized on the silica, the present one was very active. Similar results were obtained for yield and catalytic activity in the particles obtained via the acidic and basic routes.

The percentage of SiAg in the nanocomposites was calculated from the yield and the TGA residue. As the same amount of filler was always used, and the yields were similar, the SiAg content was also similar in all the nanocomposites (approximately 0.8 wt% in the first method and 1–2 wt% in the TGA residue). The concentrations of Ag in the nanocomposites were calculated by ICP-OES analysis, and showed a variation in concentration between 0.004 and 0.024 wt%. Suktha [63] used amounts of Ag from 0.001 to 0.05 wt% and obtained high antimicrobial activity. The viable cell counts of both *E. coli* and *S. aureus* were reduced by up to 99.99% at 0.05 wt% Ag loadings, indicating antimicrobial activity is possible even with low Ag concentrations.

Melting (Tm) and crystallization temperatures (Tc) and crystallinities (Xc) of the nanocomposites remained similar for the nanocomposites compared to the homogeneous polymer showing that the filler does not affect the polymer matrix thermal properties (the DSC curves are shown in Supplementary material). The onset degradation temperature was in general higher in the nanocomposites compared with neat polyethylene showing some thermal stability conferred by the filler. In general, the nanocomposites had similar or superior thermal properties compared with the neat polymer.

The morphology of the nanocomposites was studied by SEM. Fig. 3 shows the SEM images of polyethylene (a and b) and the PESiAg2 nanocomposites with silica made via the acidic (c and d) and basic (e and f) routes and polymerized by *in situ* polymerization using the non-supported method, at the same magnifications. The images show that polyethylene coats the nanoparticles, but a difference is observed in morphology between the acidic and basic routes. The morphology of the acidic route has greater structural disorder.

Fig. 4 shows the difference between the catalytic non-supported (a and b) and supported (c and d) polymerization for SiAg8 via the acidic route.

Many studies [64,65] demonstrated that the immobilization of metalocenes/methylaluminoxane (MAO) over silica occurs by the reaction of silanol groups of silica with methylaluminoxane forming a covalent bond Si—O—Al. When the metallocene is added a complexation takes place, forming ionic interactions between MAO and the metallocene which constitute the active species. It is expected that a supported catalyst would allow the polymer chains to grow from the support, replicating the nanoparticle morphology [28]. The SEM images show the different morphologies of both types of polymerization, and the supported polymerization shows a more defined morphology.

Table 5
Nanocomposites of polyethylene with SiAg. Catalytic activities and thermal properties for polymerizations using 50 mg of fillers.

Sample	Route	Polymerization	Polymer (g)	Catalytic activity (KgPE/[Zr] h bar)	SiAg T %	SiAg TGA %	Ag wt.-%	T_{onset} °C	T_{max} °C	Tc °C	Tm °C)	Xc %
PE	–	–	7.60	1689	–	0.3	–	265	496	116	133	95
PE/SiAg2	NaOH	non-supported	7.70	1711	0.8	1.2	0.004	268	495	117	134	83
PE/SiAg4			7.46	1658	0.7	2.4	0.005	276	487	117	135	84
PE/SiAg8			6.57	1460	0.8	1.9	0.024	280	492	117	133	84
PE/SiAg2		supported	6.51	8771	0.8	1.0	0.004	284	492	117	135	91
PE/SiAg4			6.65	6691	0.8	0.9	0.005	279	490	116	136	77
PE/SiAg8			5.03	6347	1.0	1.1	0.030	281	500	117	136	75
PE/SiAg2	HCOOH	non-supported	7.22	1604	0.7	2.3	0.017	269	485	117	135	95
PE/SiAg4			7.34	1631	0.7	1.9	0.017	277	502	116	133	96
PE/SiAg8			6.36	1413	0.8	1.0	0.007	290	492	118	134	88
PE/SiAg2		supported	6.53	11,315	0.8	1.3	0.019	273	484	117	134	92
PE/SiAg4			6.47	8189	0.8	1.1	0.019	288	497	116	137	89
PE/SiAg8			6.98	9770	0.7	1.4	0.006	283	499	116	137	91

All nanocomposites were tested against three bacteria, *S. aureus* (Gram positive (Fig. 5a and b)), *Salmonella* spp. (Gram negative (Fig. 5c and d), and *E. coli* (Gram negative) using Test One.

Fig. 5a, c, and e shows the discs containing the bacterial culture and 20 mm films, and Fig. 5b, d and f the discs containing the bacterial culture after 24 h, when the films were removed. It was shown that below the nanocomposite films (b and d) there was no bacterial growth, and below neat polyethylene (f) there was no bacterial inhibition.

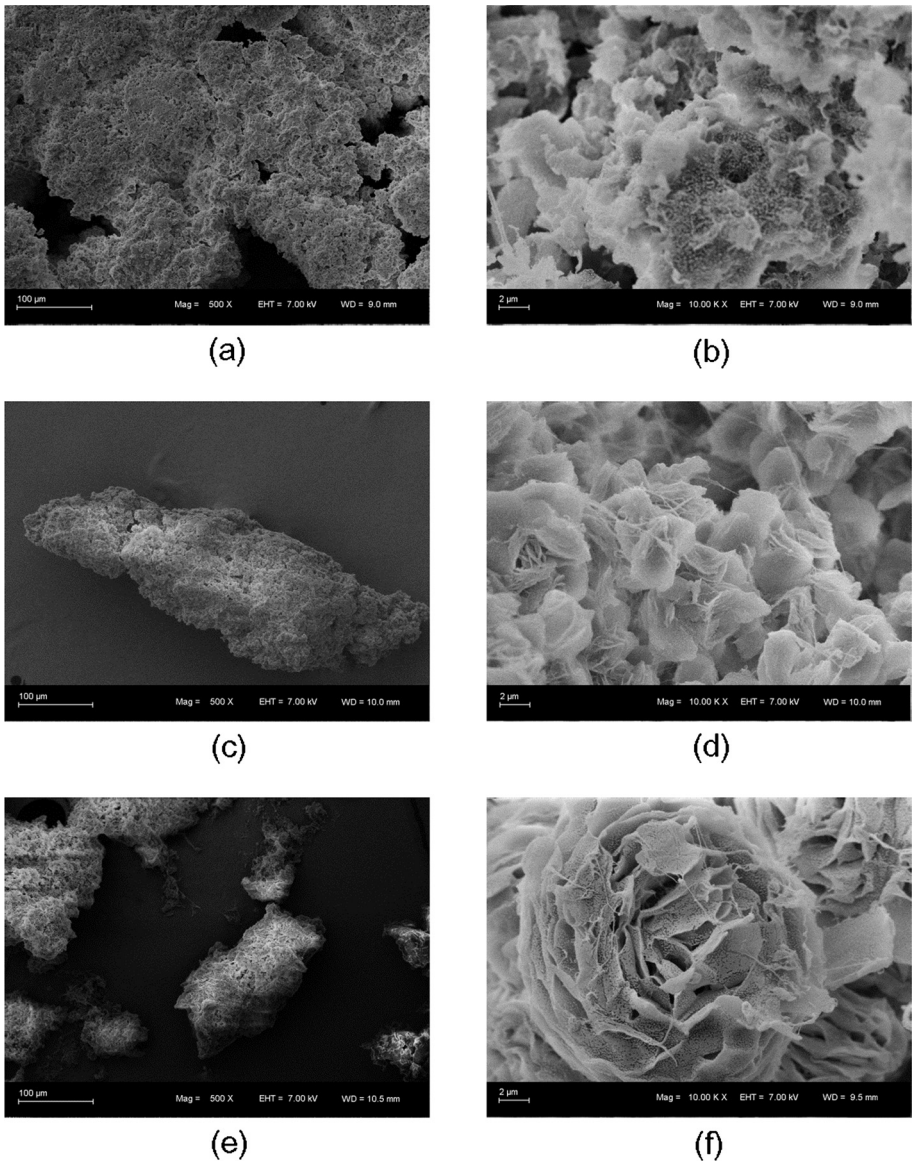

Fig. 3. SEM of (a) and (b) PE; (c) and (d) PESiAg2, non-supported, HCOOH; and (e) and (f) PESiAg2, non-supported, NaOH.

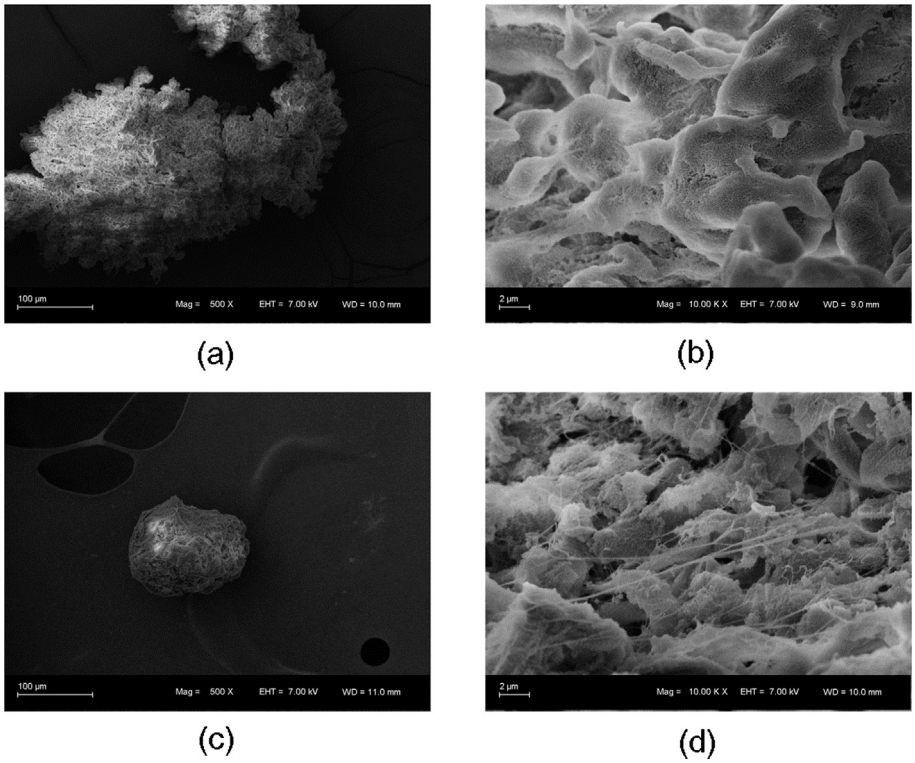

Fig. 4. SEM of (a) and (b) PESiAg8, non-supported, HCOOH; and (c) and (d) PESiAg8, supported, HCOOH.

Notably, there was no halo formation around the films. These results are of interest since they show that Ag affects bacteria only through direct contact. The nanoparticles appeared to remain in the film without lixiviation and consequent migration to the solution (AgNPs are bonded covalently to the colloidal silica and those particles are dispersed within the polymer). Despite the inability of AgNPs to migrate, and their low concentration, there is still an antimicrobial effect. This also means that the films could be used over a long period of time without losing their antibacterial effect. To assure that the inhibition under the films was not due to nanocomposites higher hydrophobicity than neat PE films, the contact angles of all the non-supported samples were obtained. The results (Table 7) showed that the nanocomposites hydrophobicity is not significant different to that of neat PE showing that the inhibition under the films it can only be attributed to the presence of the SiAg nanoparticles. These materials have potential for use in different applications, especially in the packaging industry to protect food from bacterial proliferation and to sterilize instruments. In this study, different film diameters (10 mm and 5 mm) were tested giving the same results. There were no differences between the nanocomposites obtained from the non-supported and supported polymerization or between different nanoparticles.

Test Two was carried out to measure the toxicity of the nanocomposite against *E. coli* bacteria. The effects of different nanocomposites amount on bacterial inhibition were studied. The results are shown in Table 6.

The results showed that with increasing film mass, the rate of bacterial inhibition increased. Tests for all other nanocomposites used 100 mg of film in 2 mL wells of LB liquid medium. Test Two for the nanocomposites is shown in Table 7.

The results showed that nanoparticle efficiency changed between nanocomposites. Nanoparticles (SiAg) obtained via the basic route (NaOH) had higher efficiency in controlling bacterial growth and we attributed this to the lower particle size that facilitated penetration through the bacterial membranes (the presence of a halo in Fig. 2 evidenced some particle leaching). In the nanocomposites made with SiAg obtained via the acidic route (HCOOH), the growth percentages (54–60%) of bacteria were inferior those from the SiAg obtained via the basic route (61–68% of bacterial growth). Among the nanocomposites obtained from SiAg via the acidic route, the lowest ratio (APTMS/Ag = 2) showed the highest inhibition of the growth with a value of 54%.

This can be explained by the availability of nanoparticles in the film. Test One showed that the inhibition of bacterial growth in the nanocomposites was via surface contact (there was no SiAg leaching). The active SiAg particles were those on the surface of the films that come into contact with the bacteria. This also explains why the ratio of film mass to culture medium needs to be high (100 mg for 2 mL of LB, see Table 6). Comparing the acid and basic routes, in the acidic route, the nanoparticles have a higher amount of Ag and are larger which favored surface interaction with bacteria. Comparing the reaction types (non-supported and supported), no differences were found between the methodologies for the nanoparticles obtained via the basic route, and there was a small decrease for the SiAg obtained via the acid route in the supported reaction.

4. Conclusion

Silver nanoparticles covalently bonded to a commercial silica obtained from hydrolytic condensation, with acidic or basic routes, were characterized. The acidic route produced nanoparticles with an amorphous shape, a higher concentration of silver, larger particle size, and smaller surface area compared to the basic route. There was also a difference in antibacterial activity between the two types of nanoparticles being the ones obtained via the basic route more efficient against *Escherichia coli*. As the antibacterial tests showed a halo of bacterial inhibition, it is probable that smaller particles penetrate the bacterial membranes more easily than the larger ones. Nanocomposites PE/SiAg were successfully obtained through *in situ* polymerization of ethylene using a supported and non-supported metallocene catalyst. There was a difference in the morphology of the nanocomposites obtained from the two polymerization methods, but there were no significant differences in their thermal properties.

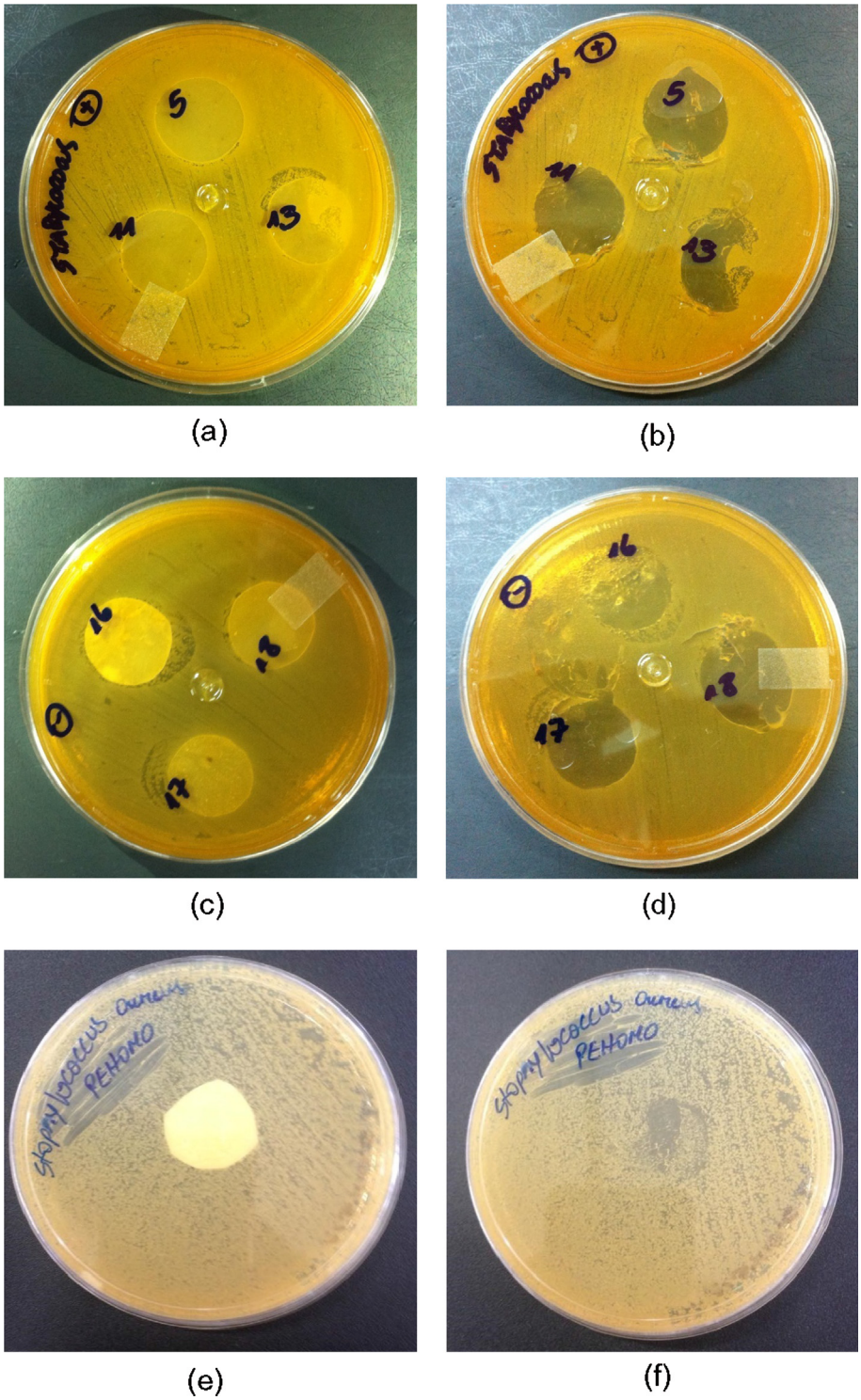

Fig. 5. Antibacterial activity of PESiAg nanoparticles tested by the disc diffusion method (test One). *(a) and (b) show 5 = PE/SiAg2NaOH supported, 11 = PE/SiAg2HCOOH supported, and 13 = PE/SiAg8HCOOH non-supported (50 mg of SiAg). **(c) and (d) show 16 = PE/SiAg8NaOH supported, 17 = PE/SiAg8HCOOH non-supported (100 mg of SiAg), and 18 = PE/SiAg8HCOOH supported (50 mg of SiAg). ***(e) and (f) show the homogeneous polymer (polyethylene).

Two antibacterial tests were carried out with each of the nanocomposites, showing no significant differences between the films obtained from the supported and non-supported polymerization. Test One was mostly qualitative and showed the antibacterial activity of all nanocomposites against *S. aureus* (Gram positive), *Salmonella* spp. (Gram negative), and *E. coli* (Gram negative). This test showed that there was no growth of bacteria below the nanocomposite film, evidencing that inhibition of bacterial growth only occurs through surface contact. Test Two (in solution) was only carried out with *E. coli*, and showed greater inhibition of bacterial growth in the presence of nanocomposites made from SiAg obtained with the acidic route, that have greater amounts of Ag and larger surface areas compared to those obtained with the basic route. The main feature of this work was the production of a thermoplastic with antibacterial properties by surface contact that could be used in packaging and in medicine.

Table 6
Antibacterial toxicity testing of PESiAg8 NaOH nanocomposite with *Escherichia coli* using test Two.

	Results	% of growth	% inhibition
Control	0.780	100	0
20 mg	0.734	94	6
40 mg	0.548	70	30
80 mg	0.477	61	39
100 mg	0.436	56	44
120 mg	0.404	52	48

Table 7
Antibacterial testing with *Escherichia coli* using 2 mL well plates and 100 mg film mass. The water contact angle is also shown.

Samples	Route	results	% of growth	WCA* (°)
CONTROL		7.29	100	
PE HOMO		7.11	98	90.4 ± 0.3
PESiAg2 HCOOH		3.95	54	78.5 ± 7.3
PESiAg4 HCOOH	non-supported	4.37	60	91.1 ± 4.9
PESiAg8 HCOOH		4.14	57	97.7 ± 1.9
PESiAg2 NaOH		4.48	61	86.0 ± 6.1
PESiAg4 NaOH	non-supported	4.71	65	75.2 ± 10.4
PESiAg8 NaOH		4.96	68	96.6 ± 2.2
PESiAg8 NaOH	supported	5.01	69	
PESiAg8 HCOOH		4.99	68	

* Water Contact angle.

Acknowledgments

The authors are grateful to Conselho Nacional de Desenvolvimento Científico e Tecnológico (CNPq) for grant 302902/2013-9 and to Coordenação de Aperfeiçoamento de Pessoal de Nível Superior (CAPES) for Giovani Pavoski grants. We also thank CME and LRNANO from UFRGS for the microscopy analysis.

References

[1] Z. Xia, Q. Ma, S. Li, D. Zhang, L. Cong, Y. Tian, R. Yang, The antifungal effect of silver nanoparticles on *Trichosporon asahii*, J. Microbiol. Immunol. Infect. 49 (2014) 182–188.
[2] N. Saifuddin, C.W. Wong, Y.A.A. Nur, Rapid biosynthesis of silver nanoparticles using culture supernatant of bacteria with microwave irradiation, E. J. Chem. 6 (2009) 61–70.
[3] J.R. Morones, J.L. Elechiguerra, A. Camacho, K. Holt, J.B. Kouri, J.T. Ramírez, et al., The bactericidal effect of silver nanoparticles, Nanotechnology 10 (2005) 2346–2353.
[4] J.A. Dahl, B.L. Maddux, J.E. Hutchison, Toward greener nanosynthesis, Chem. Rev. 107 (2007) 2228–2269.
[5] D. Ito, M.L. Jespersen, J.E. Hutchison, Selective growth of vertical ZnO nanowire arrays using chemically anchored gold nanoparticles, ACS Nano 2 (2008) 2001–2006.
[6] S. Egger, R.P. Lehmann, M.J. Height, M.J. Loessner, M. Schuppler, Antimicrobial properties of a novel silver-silica nanocomposite material, Appl. Environ. Microbiol. 75 (2009) 2973–2976.
[7] F.C. Fim, J.M. Guterres, N.R.S. Basso, G.B. Galland, Polyethylene/graphite nanocomposites obtained by *in situ* polymerization, J. Polym. Sci. A 48 (2010) 692–698.
[8] M.A. Milani, R. Quijada, N.R.S. Basso, A.P. Graebin, G.B. Galland, Influence of the graphite type on the synthesis of polypropylene/graphene nanocomposites, J. Polym. Sci. A 50 (2012) 3598–3605.
[9] F.C. Fim, N.R.S. Basso, A.P. Graebin, D.S. Azambuja, G.B. Galland, Thermal, electrical, and mechanical properties of polyethylene–graphene nanocomposites obtained by *in situ* polymerization, J. Appl. Polym. Sci. 128 (2012) 2630–2637.
[10] M. Nisar, P.S. Thue, C.A. Heck, J.L. Salazar Cuaila, J. Geshev, E.C. Lima, M.M. Jacobi, G.B. Galland, Synthesis of polyethylene/nickel-carbon stimuli-responsive material under magnetic field at room temperature: Effect of the filler on the properties, Eur. Polym. J. 99 (2018) 378–383.
[11] P. Dallas, V.K. Sharma, R. Zboril, Silver polymeric nanocomposites as advanced antimicrobial agents: classification, synthetic paths, applications, and perspectives, Adv. Colloid Interface Sci. 166 (2011) 119–135.
[12] H. Münstedt, K.C. Radhesh, Silver ion release antimicrobial polyamide/silver composites, Biomaterials 26 (2005) 2081–2088.
[13] M.N. Alekshun, S.B. Levy, Molecular mechanisms of antibacterial multidrug resistance, Cell 28 (2007) 1037–1050.
[14] A. Bubnoff, Seeking new antibiotics in Nature's backyard, Cell 127 (2006) 867–869.
[15] M.F. Maitz, Applications of synthetic polymers in clinical medicine, Biosurface Biotribol. 1 (2015) 161–176.
[16] H. Cao, X. Liu, Silver nanoparticles-modified films versus biomedical device associated infections, Wiley Interdiscip. Rev. Nanomed. Nanobiotechnol. 2 (2010) 670–684.
[17] W.G.I.U. Rathnayake, H. Ismail, A. Baharin, A.G.N.D. Darsanasiri, S. Rajapakse, Synthesis and characterization of nano silver based natural rubber latex foam for imparting antibacterial and anti-fungal properties, Polym. Test. 31 (2012) 586–592.
[18] I. Sondi, B. Salopek-Sondi, Silver nanoparticles as antimicrobial agent: a case study on *E. coli* as a model for Gram-negative bacteria, J. Colloid Interface Sci. 275 (2004) 177–182.
[19] Y. Li, P. Leung, L. Yao, Q. Song, E. Newton, Antimicrobial effect of surgical masks coated with nanoparticles, J. Hosp. Infect. 62 (2006) 58–63.
[20] W.K. Son, J.H. Youk, W.H. Park, Antimicrobial cellulose acetate nanofibers containing silver nanoparticles, Carbohydr. Polym. 65 (2006) 430–434.
[21] J.S. Kim, E. Kuk, K.N. Yu, J.H. Kim, S.J. Park, H.J. Lee, S.H. Kim, Y.K. Park, Y.H. Park, C.Y. Hwang, Antimicrobial effects of silver nanoparticles, Nanomedicine 3 (2007) 95–101.
[22] L.A. Tamayo, P.A. Zapata, N.D. Vejar, M.I. Azócar, M.A. Gulppi, X. Zhouc, G.E. Thompson, F.M. Rabagliati, M.A. Páez, Release of silver and copper nanoparticles from polyethylene nanocomposites and their penetration into Listeria monocytogenes, Mater. Sci. Eng. C 40 (2014) 24–31.
[23] Y. Zheng, J. Miao, F. Zhang, C. Cai, A. Koh, T.J. Simmons, S.A. Mousa, R.J. Linhardt, Surface modification of a polyethylene film for anticoagulant and antimicrobial catheter, React. Funct. Polym. 100 (2016) 142–150.
[24] S.A. Kulkarni, B.A. Kakade, I.S. Mulla, V.K. Pillai, Suppression of electron-transfer characteristics of ferrocene by OTS monolayer on a silicon/electrolyte interface, J. Colloid Interface Sci. 299 (2006) 777–784.
[25] I.E. dell'Erba, A.Y. Mansilla, C.E. Hoppe, R.J.J. Williams, Synthesis and characterization of an antibacterial powder based on the covalent bonding of aminosilane-stabilized silver nanoparticles to a colloidal silica, J. Mater. Sci. 51 (2016) 3817–3823.
[26] Z. Hu, C. Liu, Z. Hu, C. Liu, Polyethylene/graphite oxide nanocomposites obtained by in situ polymerization using modified graphite oxide–supported metallocene catalysts, J. Polym. Res. 20 (2013) 39.
[27] L. Guo, W. Yuan, Z. Lua, C.M. Li, Polymer/nanosilver composite coatings for antibacterial applications, Colloids Surf. A 439 (2013) 69–83.
[28] G. Dacarro, L. Cucca, P. Grisoli, P. Pallavicini, M. Patrini, A. Taglietti, Monolayers of polyethilenimine on flat glass: a versatile platform for cations coordination and nanoparticles grafting in the preparation of antibacterial surfaces, Dalton Trans. 41 (2012) 2456–2463.
[29] G. Pavoski, T. Maraschin, M.A. Milani, D.S. Azambuja, R. Quijada, C.S. Moura, N.S. Basso, G.B. Galland, Polyethylene/reduced graphite oxide nanocomposites with improved morphology and conductivity, Polymer 81 (2015) 79–86.
[30] W. Kaminsky, A. Funck, H. Hähnsen, New application for metallocene catalysts in olefin polymerization, Dalton Trans. 41 (2009) 8803–8810.
[31] A. Michael, G. Beyer, C. Henrist, R. Cloots, A. Rulmont, R. Jérôme, P. Dubois, Preparation and properties of layered silicate nanocomposites based on ethylene vinyl acetate copolymers, Macromol. Rapid. Commun. 22 (2001) 643–646.
[32] A. Michael, M. Pluta, P. Dubois, R. Jérôme, Metallocene catalyzed polymerization of ethylene in the presence of graphite, 1. Synthesis and characterization of the composites, Macromol. Chem. Phys. 202 (2001) 2239–2246.
[33] M. Alexandre, T. Sun, J. Garces, R. Jérôme, P. Dubois, Polyethylene-layered silicate nanocomposites prepared by the polymerization-filling technique: synthesis and mechanical properties, Polymer 43 (2002) 2123–2132.
[34] F. Silveira, M.C.M. Alves, F.C. Stedile, S.B. Pergherb, A. Rigacci, J.H.Z. Santos, Effect of the silica texture on the structure of supported metallocene catalysts, J. Mol. Catal. A Chem. 298 (2009) 40–50.
[35] J.R. Severn, J.C. Chadwick, R. Duchateau, N. Friederichs, "Bound but not gagged" immobilizing single-site α-olefin polymerization catalysts, Chem. Rev. 105 (2005) 4073–4147.
[36] H. Hammawa, S.E. Wanke, Influence of support friability and concentration of α-olefins on gas-phase ethylene polymerization over polymer-supported metallocene/methylaluminoxane catalysts, J. Appl. Polym. Sci. 104 (2007) 514–527.
[37] M.W. McKittrici, C.W. Jones, Modulating the reactivity of an organometallic catalyst via immobilization on a spatially patterned silica surface, Chem. Mater. 17 (2005) 4758–4761.
[38] R.M. Kasi, E.B. Coughlin, Supported constrained-geometry catalysts on cross-linked (aminomethyl)polystyrene: studies of ethylene and 1-octene polymerizations, Organometallics 22 (2003) 1534–1539.
[39] S.L. Burkett, S. Soukasene, K.L. Milton, R. Welch, A.J. Little, R.M. Kasi, E.B. Coughlin, Tethered constrained-geometry catalysts in mesoporous silica: probing the influence of the "second sphere" on polymer properties, Chem. Mater. 17 (2005) 2716–2723.
[40] G.G. Hlatky, J. Scheirs, W. Kaminsky, Metallocene-based Polyolefins, Wiley, West Sussex, UK, 2000, pp. 201–218.
[41] G.B. Galland, M. Seferin, R.S. Mauler, J.H.Z. Santos, Linear low-density polyethylene synthesis promoted by homogeneous and supported catalysts, Polym. Int. 48 (1999) 660–664.
[42] G.B. Galland, J.H.Z. Santos, F.C. Stedile, P.P. Greco, A.D. Campani, Evaluation of silica-supported zirconocenes in ethylene/1-hexene copolymerization, J. Mol. Catal. A Chem. 210 (2004) 149–156.
[43] D. Bianchini, G.B. Galland, J.H.Z. Santos, D.P. Fasce, I.E. Dell'Erba, R. Quijada,

M. Perez, Metallocene supported on a polyhedral oligomeric silsesquioxane-modified silica with high catalytic activity for ethylene polymerization, J. Polym. Sci. A Polym. Chem. 43 (2005) 5465–5476.
[44] W. Amarego, D. Perrin, Purification of Laboratory Chemicals, fourth ed., Linacre Hause, USA, 1997.
[45] N. Plumer, A. Ruff, B. Speiser, V. Feldmann, H.A. Mayer, Stöber silica particles as basis for redox modifications: particle shape, size, polydispersity, and porosity, J. Colloid Interface Sci. 368 (2012) 208–219.
[46] S.R. Kline, Reduction and analysis of SANS and USANS data using IGOR Pro, J. Appl. Crystallogr. 39 (2006) 895–900.
[47] C.J. Brinker, G.W. Scherer, Sol–Gel Science: The Physics and Chemistry of Sol–Gel Processing, Academic Press, San Diego, USA, 1990, pp. 97–284.
[48] S. Brunauer, P.H. Emmett, E. Teller, Adsorption of gases in multimolecular layers, J. Am. Chem. Soc. 60 (1938) 309–319.
[49] M. Jafarzadeh, I.A. Rahman, C.S. Sipaut, Synthesis of silica nanoparticles by modified sol–gel process: the effect of mixing modes of the reactants and drying techniques, J. Sol-Gel Sci. Technol. 50 (2009) 328–336.
[50] E.P. Barrett, L.G. Joyner, P.P. Halenda, The determination of pore volume and area distributions in porous substances. I. Computations from nitrogen isotherms, J. Am. Chem. Soc. 73 (1951) 373–380.
[51] J. Minick, A. Moet, E. Baer, Morphology of HDPE/LDPE blends with different thermal histories, Polymer 36 (1995) 1923–1932.
[52] G. Sezonov, D. Joseleau-Petit, R. D'Ari, *Escherichia coli* physiology in Luria-Bertani broth, J. Bacteriol. 189 (2007) 8746–8749.
[53] E.F. Vansant, P. Van Der Voort, K.C. Vrancken, Characterization and Chemical Modification of the Silica Surface, Elsevier, Amsterdam, 1995.
[54] F. Lu, S.H. Wu, Y. Hung, C.Y. Mou, Size effect on cell uptake in well-suspended, uniform mesoporous silica nanoparticles, Small 5 (2009) 1408–1413.
[55] Z.A. Qiao, L. Zhang, M.Y. Guo, Y.L. Liu, Q.S. Huo, Synthesis of mesoporous silica nanoparticles via controlled hydrolysis and condensation of silicon alkoxide, Chem. Mater. 21 (2009) 3823–3829.
[56] Y.P. Moreno, M.B. Cardoso, E.A. Moncada, J.H.Z. Santos, Correlating the morphological properties and structural organization of monodisperse spherical silica nanoparticles grown on a commercial silica surface, Chem. Phys. Chem. 16 (2015) 2981–2994.
[57] G. Beaucage, H.K. Kammler, S.E. Pratsinis, Particle size distributions from small-angle scattering using global scattering functions, J. Appl. Crystallogr. 37 (2004) 523–535.
[58] G. Beaucage, Small-angle scattering from polymeric mass fractals of arbitrary mass-fractal dimension, J. Appl. Crystallogr. 29 (1996) 134–146.
[59] G. Beaucage, Approximations leading to a unified exponential/power-law approach to small-angle scattering, J. Appl. Crystallogr. 28 (1995) 717–728.
[60] G.J. Owens, R.K. Singh, F. Foroutan, M. Alqaysi, C. Han, C. Mahapatra, H. Kim, J.C. Knowles, Sol-gel based materials for biomedical applications, Prog. Mater. Sci. 77 (2016) 1–79.
[61] A.A. Bernardes, C. Radtke, M.C.M. Alves, I.M. Baibich, M. Lucchese, J.H.Z. dos Santos, Synthesis and characterization of SiO2–CrO3, SiO2–MoO3, and SiO2–WO3 mixed oxides produced using the non-hydrolytic sol–gel process, J. Sol-Gel Sci. Technol. 69 (2014) 72–84.
[62] M. Thommes, K. Kaneko, A.V. Neimark, J.P. Olivier, F. Rodriguez-Reinoso, J. Rouquerol, K.S.W. Sing, Physisorption of gases, with special reference to the evaluation of surface area and pore size distribution (IUPAC Technical Report), Pure Appl. Chem. 87 (2015) 1051–1069.
[63] P. Suktha, K. Lekpet, P. Siwayaprahm, M. Sawangphruk, Enhanced mechanical properties and bactericidal activity of polypropylene nanocomposite with dual-function silica–silver core-shell nanoparticles, J. A ppl. Polym. 128 (2013) 4339–4345.
[64] W. Kaminsky, Differences in activities and polymer microstructures by supporting metallocene catalysts, Kinet. Catal. 47 (2006) 221–226.
[65] F. Ciardelli, A. Altomare, M. Michelotti, From homogeneous to supported metallocene catalysts, Catal.Today 41 (1998) 149–157.